A Comparison of Two Soil Moisture Products S^{2}MP and Copernicus-SSM Over Southern France

Hassan Bazzi, Nicolas Baghdadi, Mohammad El Hajj, Mehrez Zribi, and Hatem Belhouchette

***Abstract*—This paper presents a comparison between the Sentinel-1/Sentinel-2-derived soil moisture product at plot scale (S^{2}MP) and the new Copernicus surface soil moisture (C-SSM) product at 1-km scale over a wide region in southern France. In this study, both products were first evaluated using *in situ* measurements obtained by the calibrated time delay reflectometer in field campaigns. The accuracy against the *in situ* measurements was defined by the correlation coefficient *R*, the root mean square difference (RMSD), and the bias and the unbiased root mean square difference (ubRMSD). Then, the soil moisture estimations from both SSM products were intercompared over one year (October 2016–October 2017). Both products show generally good agreement with *in situ* measurements. The results show that using *in situ* measurements collected over agricultural areas and grasslands, the accuracy of the C-SSM is good (RMSD = 6.0 vol%, ubRMSD = 6.0 vol%, and $R = 0.48$) but less accurate than the S^{2}MP (RMSD = 4.0 vol%, ubRMSD = 3.9 vol%, and $R = 0.77$). The intercomparison between the two SSM products over one year shows that both products are highly correlated over agricultural areas that are mainly used for cereals (*R* value between 0.5 and 0.9 and RMSE between 4 and 6 vol%). Over areas containing forests and vineyards, the C-SSM values tend to overestimate the S^{2}MP values (bias > 5 vol%). In the case of well-developed vegetation cover, the S^{2}MP does not provide SSM estimations while C-SSM sometimes provides underestimated SSM values.**

***Index Terms*—Copernicus surface soil moisture (SSM), Sentinel-1 soil moisture, soil moisture product at plot scale (S^{2}MP), South France.**

I. Introduction

UNDERSTANDING the water cycle and climate change requires the spatial and temporal monitoring of the surface soil moisture (SSM) [1]. The spatiotemporal monitoring of soil moisture is important in the fields of hydrology, climatology, and agronomy [2], [3]. For example, monitoring natural phenomena, such as drought and floods, requires continuous soil moisture data because soil moisture is a key variable in the global water cycle. Moreover, soil moisture data at high spatial resolution is essential for agricultural management, such as monitoring of irrigation practices and water requirements of agricultural areas [4]–[7]. Therefore, continuous soil moisture data at both high spatial and temporal resolutions are important for many hydrological and agricultural models.

To estimate soil moisture, synthetic aperture radar (SAR) data are widely used in both C- and X-bands. Soil moisture values are mainly obtained through the inversion of either physical [8], [9] or statistical models [10]–[12]. While statistical models require site calibration, physical models can always be used to simulate the radar backscattering from radar configuration. Among the physical models, the integral equation model (IEM) [9] is the most commonly used to estimate soil moisture over bare soil or soil with little vegetation cover. Baghdadi *et al.* [13], [14] proposed a semiempirical calibration of the IEM to compensate between the large difference observed between IEM simulation and real SAR data. To estimate soil moisture over vegetated areas, the water cloud model (WCM) developed by Attema and Ulaby [15] is commonly used. In the WCM, the radar backscattering signal is modeled as a sum of the direct vegetation contribution and the soil contribution multiplied by the attenuation factor. Several studies have parametrized the WCM for different SAR band configurations and for several crop types [5], [16]. In addition to the inversion of statistical or physical models for soil moisture retrieval, recent studies have started reporting the estimation of soil moisture using the change detection method. In this method, the change in backscattering coefficients between two successive dates is linked to the change in soil moisture values where vegetation and roughness are considered stable [17]–[19]. Currently, several satellite missions provide SSM estimations at different spatial resolutions: the soil moisture active passive (SMAP) (level 3: 36 km × 36 km, level 3 enhanced: 9 km × 9 km, and level 2 SMAP/Sentinel-1: 1 km × 1 km) [20], the advanced scatterometer (ASCAT) (level 2 with three spatial resolution 25 km × 25 km, 12.5 km × 12.5 km, and 1 km × 1 km) [21], and the soil moisture and ocean salinity (SMOS) (SMOS INRA-CESBIO level 3: 25 km × 25 km) [22]. However, the low spatial resolution is not adequate for water cycle monitoring and for agricultural management at plot scale.

Recently, the arrival of the Sentinel-1 (S1) SAR satellite provided users with free open access SAR data at a high spatial

Manuscript received March 12, 2019; revised June 18, 2019; accepted June 28, 2019. Date of publication September 25, 2019; date of current version September 29, 2019. This work was supported in part by the French Space Study Center (2019 TOSCA) and in part by the National Research Institute of Science and Technology for Environment and Agriculture (IRSTEA). *(Corresponding author: Hassan Bazzi.)*

H. Bazzi, N. Baghdadi, and M. El Hajj are with the National Research Institute of Science and Technology for Environment and Agriculture, TETIS, University of Montpellier, 34093 Montpellier cedex 5, France (e-mail: hassan.bazzi@irstea.fr; nicolas.baghdadi@teledetection.fr; mohammad.el-hajj@teledetection.fr).

M. Zribi is with the Centre d'Etudes Spatiales de la Biosphère (CNRS/UPS/IRD/CNES/INRA), 31401 Toulouse cedex 9, France (e-mail: mehrez.zribi@ird.fr).

H. Belhouchette is with CIHEAM-IAMM, UMR-System, 34090 Montpellier, France (e-mail: belhouchette@iamm.fr).

Digital Object Identifier 10.1109/JSTARS.2019.2927430

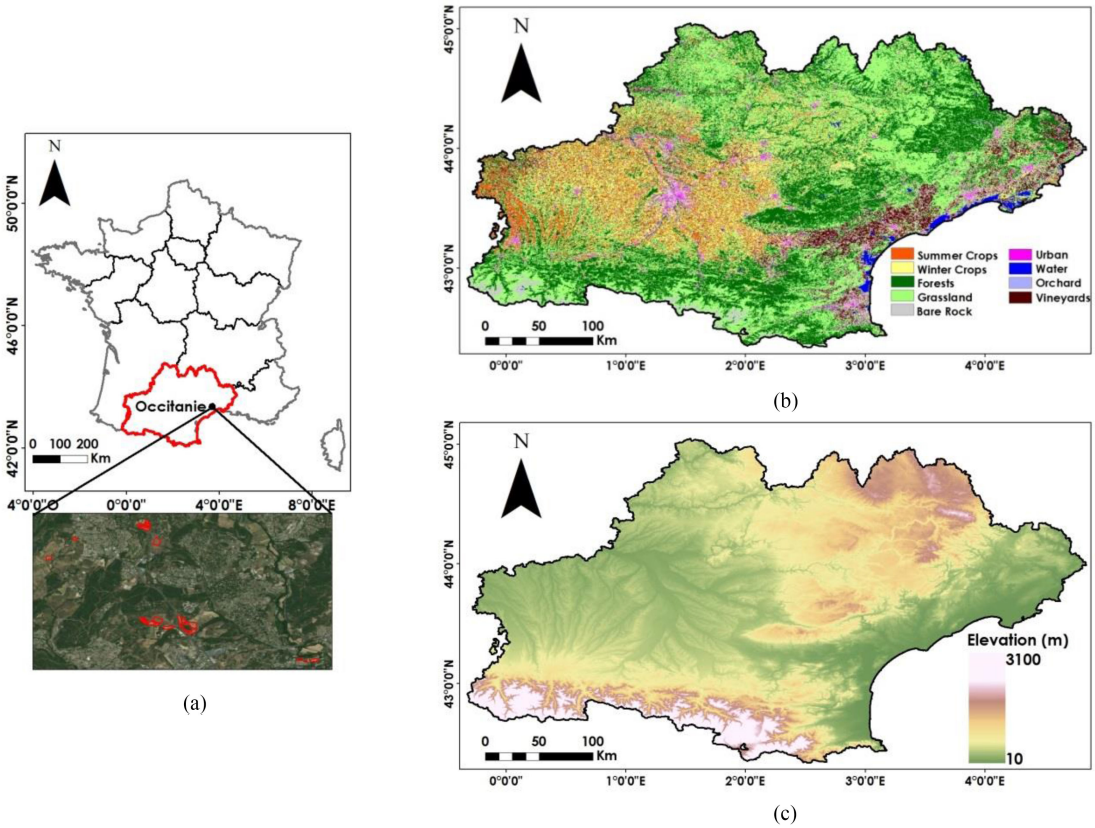

Fig. 1. (a) Location of the Occitanie region, South France, with the *in situ* reference plots. (b) Land cover map of Occitanie produced by Theia (http://www.theia-land.fr/en/thematic-products). (c) Elevation derived from the SRTM DEM of 30-m spatial resolution.

resolution (10 m × 10 m) and high revisit time (six days over Europe). The S1 mission from the European Space Agency is a constellation of two polar orbiting SAR satellites (Sentinel-1A and Sentinel-1B) operating in the C-band (∼5.4 GHz). The S1A and S1B SAR sensors operate in four acquisition modes: strip map, interferometric wide swath (IW), extrawide swath (EW), and wave (WV). Among the four modes, the IW mode provides images with a spatial resolution of 10 m × 10 m. The SAR data of the S1 mission at high spatial and temporal resolutions have encouraged mapping soil moisture in an operational mode. Paloscia *et al*. [12] used the neural network (NN) technique to invert the Sentinel-1 SAR C-band and estimate the SSM values. Mattia *et al*. [17] estimated soil moisture at 1 km × 1 km spatial resolution using the change detection technique applied to Sentinel-1 SAR time series. Recently, El Hajj *et al*. [23] developed an operational method to map soil moisture at the plot scale over agricultural areas based on coupling S1-SAR data and Sentinel-2 (S2) optical data using the NN technique. The synergic use of S1 and S2 data allowed the provision of soil moisture product at the plot scale (S^{2}MP) for several sites over the world (South France, Lebanon, etc.) Most recently, the Copernicus Global Land Service has started providing SSM of the soil's topmost 5 cm over the European continent from Sentinel-1 sensors at 1 km × 1 km spatial resolution using the change detection method [24].

The objective of this study is to evaluate the performance of the Copernicus SSM (C-SSM) product and S^{2}MP product over a wide region in South France. In this study, both products are first evaluated against *in situ* measurements of soil moisture. The new Copernicus SSM product was then intercompared with the SSM estimations from the S^{2}MP. The correlation between the products was analyzed as a function of the land cover. Section II presents the SSM products used, the *in situ* SSM measurements, and the applied methods. The results and discussions are presented in Section III. Finally, Section IV presents the main conclusions.

II. Materials and Methods

A. Study Site

The study site examined is the Occitanie region of southern France (centered on 2°30′E and 43°30′N, Fig. 1), with an area of 72 724 km^2 [see Fig. 1(a)]. Fig. 1(b) presents the land cover of the studied region derived from the land cover map produced by Inglada *et al*. [25] and made available via the Theia French Land Data Center (http://www.theia-land.fr/en/thematic-products). The region has a variety of landscape and is mainly covered by agricultural areas in the middle and western parts. The northern regions are generally covered with a mix of forests,

grassland and agricultural crop land. The eastern region is generally covered with a mix of agricultural crop land, grassland, and vineyards. Fig. 1(c) shows the elevations derived from the digital elevation model (DEM) of the Shuttle Radar Topography Mission (SRTM) at a 1 arc-second spatial resolution (∼30 m). The climate in the eastern part of the region is considered Mediterranean (approximately 700 mm average annual precipitation), whereas that of the western part is more humid and oceanic (approximately 1200 mm average annual precipitation) (http://www.meteofrance.com/climat/france/).

B. In Situ Soil Moisture Measurements

Over an area near Montpellier, France [see Fig. 1(a)], the SSM values were measured on 23 reference plots (10 grassland and 13 wheat) during the period between January 1, 2017 and May 31, 2017 [23]. The SSM values were measured within 2 h of the S1 acquisition time in 22 different campaigns at different dates of S1 acquisition. For each plot, 25–30 volumetric soil moisture measurements were taken from the top 5 cm layer using a calibrated time delay reflectometer (TDR). Then, within each plot, the SSM measurements were averaged to obtain a mean value for each plot. The measured soil moisture values varied between 7.0 and 36.3 vol%.

C. S^2MP Product

The S^2MP product is obtained by coupling Sentinel-1 SAR data and Sentinel-2 optical data. The S^2MP product provides SSM estimates over the agricultural areas at plot scale with six days revisit time [23]. To estimate the SSM values, El hajj *et al*. [23] inverted the WCM parameterized by Baghdadi *et al*. [26] for C-band combined with the IEM, as modified by Baghdadi *et al*. [13]. The inversion approach uses the NN technique to invert the radar signal into SSM value. To operationally map the soil moisture, the developed NN uses the C-band SAR signal in VV polarization, SAR incidence angle, and the normalized differential vegetation index (NDVI) as the inputs. While the SAR signal and incidence angle are derived from the S1 data, the NDVI value is derived from Sentinel-2 images. To overcome the cloud limit usually present in optical images, one NDVI image each month is usually used to obtain the NDVI value required for the inversion. The S^2MP maps are produced for agricultural areas (it is not applied to vineyards and orchards). Forest and urban areas are masked using the land cover map of Inglada *et al*. [25]. Additionally, areas with slope greater than 20% are masked in the soil moisture product (calculated from SRTM DEM at 30-m spatial resolution). The S^2MP are available in free open access mode via the Theia French Land Data Center (http://www.theia-land.fr/en/thematic-products). In this study, only the S^2MP maps for images in ascending mode were produced and compared to *in situ* and C-SSM data for two main reasons. First S1 images in descending mode are acquired at 05:40 UT with a high probability of freeze in winter causing an underestimation of SSM [27]. Second, *in situ* measurements were acquired within 2 h of the ascending S1 acquisitions. Thus, our *in situ* measurements could be not applicable to SSM estimations obtained from S1 images in descending mode.

D. Copernicus SSM product

Recently, Copernicus Global Land Service began to distribute the first soil moisture estimations over the European continent at a 1-km spatial resolution using S1 data in C-band [24]. The SSM retrieval algorithm is based on the TU (University of Technology) Wien Change Detection Model already applied for the ASCAT data and adapted for Sentinel-1 data. In the applied model, the changes observed in the SAR backscattered coefficient (σ^0) are interpreted as changes in the soil moisture values, whereas other surface properties such as the geometry, the surface roughness, and the vegetation cover are interpreted as static parameters. To estimate relative SSM at time t (SSM_t) in percent (%), the backscattered coefficient $\sigma^0(\theta, t)$ observed at time t with a given SAR incidence angle θ is normalized to a reference angle Θ and linearly scaled between dry and wet reference values

$$\mathrm{SSM}_t = \frac{\Delta\sigma^0(\Theta, t)}{S(\Theta)}\,[\%] \tag{1}$$

where $\Delta\sigma^0(\Theta, t)$ is the change in the normalized backscatter (relative to dry conditions), and $S(\Theta)$ is the sensitivity to the SSM changes at reference angle $\Theta = 40^\circ$, expressed as follows:

$$S(\Theta) = {\sigma^0}_{\mathrm{wet}}(\Theta) - {\sigma^0}_{\mathrm{dry}}(\Theta)\ \ [\mathrm{dB}] \tag{2}$$

where ${\sigma^0}_{\mathrm{wet}}(\Theta)$ and ${\sigma^0}_{\mathrm{dry}}(\Theta)$ are the highest and lowest backscattered values at the individual location, respectively.

The C-SSM products at 1-km spatial resolution are retrieved from the Sentinel-1 radar backscattering images acquired in IW mode and VV polarization. The product delivers relative SSM values in percentages ranging between 0% and 100%. In the case of extremely dry conditions, frozen soil, snow-covered soil, and flooding, the C-SSM retrieval is ill posed. In these cases, the C-SSM does not provide estimation, and it encodes values of 241 and 242 in the product. Moreover, the product masks water surfaces (sea, lakes, rivers, etc.), urban areas, and dense forests with values equal to 252. High undulating terrains with slopes greater than 30% are also masked in the product and encoded as 253.

The C-SSM product values were converted to a volumetric unit (vol%) in order to compare the C-SSM estimations produced in relative units (%), with measured soil moisture being given in absolute volumetric unit (vol%). Thus, the C-SSM values were converted to vol% unit (SSM_α) by using the 90% confidence interval of a Gaussian distribution [28] equal to $\mu + 1.65\sigma$, where μ and σ are the mean and the standard deviation of the TDR ground data

$$\mathrm{SSM}_\alpha(t) = \mathrm{SSM}(t) \times (\mathrm{SSM}_{\max} - \mathrm{SSM}_{\min}) + \mathrm{SSM}_{\min} \tag{3}$$

where $\mathrm{SSM}_\alpha(t)$ is the volumetric SSM at a time t (in vol%), $\mathrm{SSM}(t)$ is the relative C-SSM soil moisture content (in %), $\mathrm{SSM}_{\max}$ is the maximum measured wetness value (in vol%) equal to $\mu + 1.65\sigma$, and $\mathrm{SSM}_{\min}$ is the minimum measured wetness value (in vol%) equal to $\mu - 1.65\sigma$. Using the *in-situ* measured soil moisture values, $\mathrm{SSM}_{\max} = 39.7\,\mathrm{vol}\%$ and $\mathrm{SSM}_{\min} = 7.5\,\mathrm{vol}\%$.

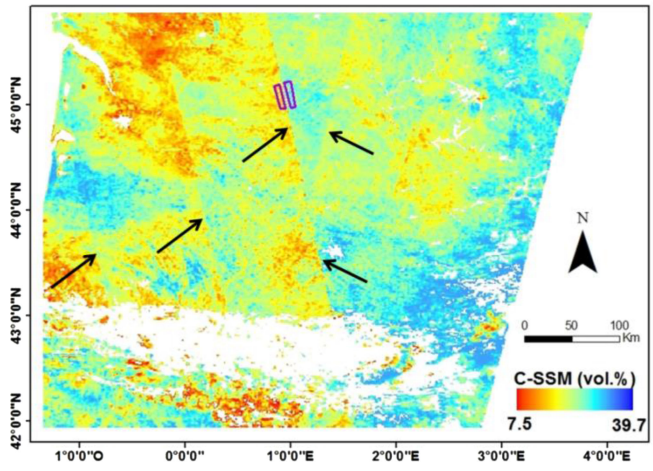

Fig. 2. C-SSM product over South France. White areas represent the mask applied in the C-SSM product. Arrows are used to highlight the discontinuity observed between the subswaths with the C-SSM product. Magenta polygons are used to calculate the C-SSM mean value at the subswath limits.

Fig. 2 shows an example of the C-SSM product covering a part of southern France on 25/03/2017. The physical soil moisture values of the C-SSM product are converted to volumetric units (vol%). Strong discontinuities are observed in the C-SMM product between the different subswaths of Sentinel-1 SAR data (black arrows). As an example, the statistical mean calculated for the two magenta polygons in Fig. 2 (at both sides of the two subswaths) shows that the difference in SSM estimates is 11 vol%.

E. Methods

Since the C-SSM product is produced at a 1-km spatial resolution, and the S^{2}MP product is produced at the plot scale, the evaluation was carried out at a 1 km $\times$ 1 km spatial resolution (the same grid of the C-SSM product). For each field campaign, the *in situ* soil moisture measurements carried out on all plots within the same 1 km $\times$ 1 km of the C-SSM grid cell were averaged. Moreover, the S^{2}MP product was also aggregated by averaging the high-resolution soil moisture pixels of S^{2}MP within each C-SSM cell of 1 km $\times$ 1 km. This means that, at a given date, for each C-SSM cell (1 km $\times$ 1 km) the values of the S^{2}MP estimations within the cell were averaged to obtain a 1 km $\times$ 1 km S^{2}MP value. Therefore, for each available S^{2}MP map, the mean soil moisture values were calculated for the corresponding C-SSM grid.

First, S^{2}MP and C-SSM were evaluated by comparing SSM values from each product (at 1-km spatial resolution) with the *in situ* soil moisture, which were also averaged at 1-km C-SSM grid cell. Since both SSM products have been produced at different temporal resolution (in this study S^{2}MP was applied only on S1 acquisitions in ascending mode whereas that C-SSM was generated for all S1 overpasses), only those SSM maps with common dates between S^{2}MP, C-SSM, and *in situ* campaigns were considered in the comparison. Thus, the sample size used for the comparison is the same for both SSM products. The accuracy of the products was determined using the statistical metrics including the Pearson correlation coefficient (R), the root mean square difference (RMSD), the bias (estimated SSM–measured SSM), and the unbiased root mean square difference (ubRMSD). These metrics are calculated as follows:

$$R = \frac{\sum_{i=1}^{n}\left[\left(O_i-\bar{O}\right)\left(P_i-\bar{P}\right)\right]}{\sqrt{\sum_{i=1}^{n}\left(O_i-\bar{O}\right)^2}\sqrt{\sum_{i=1}^{n}\left(P_i-\bar{P}\right)^2}} \tag{4}$$

$$\mathrm{RMSD} = \sqrt{\frac{1}{n}\sum_{i=1}^{n}\left(O_i-P_i\right)^2} \tag{5}$$

$$\mathrm{Bias} = \frac{1}{n}\sum\left(O_i-P_i\right) \tag{6}$$

$$\mathrm{ubRMSD} = \sqrt{\mathrm{RMSD}^2-\mathrm{Bias}^2} \tag{7}$$

where P_i is the *in situ* measurement at grid cell i, O_i is the SSM product estimation at grid cell i, $\bar{P}$ is the average value of the *in situ* measurements at all compared grid cells, and $\bar{O}$ is the average value of the SSM product estimation at all grid cells. The four statistical metrics were calculated for each product. The obtained results are presented in Section III-A.

Then, an intercomparison was performed between the S^{2}MP and the C-SSM products over the entire Occitanie region for the period between October 1, 2016 and October 1, 2017 using the statistical metrics R, RMSD, bias, and ubRMSD. The intercomparison was performed at each grid cell using SSM estimates over one year. Since the two products have a different temporal resolution, only those SSM values with common dates between the S^{2}MP and C-SSM were considered in the intercomparison. The same grid of C-SSM was used for the regridding of S^{2}MP. For each C-SSM cell (1 km $\times$ 1 km), the S^{2}MP SSM estimations existing within the C-SSM cell were averaged to obtain a 1 km $\times$ 1 km S^{2}MP value. The statistical metrics were not calculated for those cells where the S^{2}MP product or the C-SSM product does not provide soil moisture estimation over the entire year due to the applied masks. Four maps, each representing one of the statistical metrics, are presented and discussed in Section III-B.

Finally, the temporal evolution of the soil moisture estimations derived from both SSM products was investigated. This temporal evolution was performed for one wheat and one maize grid cell (the cell is predominantly covered by wheat and maize, respectively). Temporal profiles are further presented in Section III-C.

III. Results and Discussion

A. Comparison Between SSM Products and In Situ SSM

The SSM values of each product were evaluated using the *in situ* SSM measurements during the period between January 2017 and May 2017. Fig. 3 shows the comparison between the SSM products and the *in situ* SSM measurements, whereas Table I summarizes the statistical metrics obtained from the comparison of each product with the *in situ* measurements. In general, the accuracy of the S^{2}MP product is higher than that of the Copernicus SSM. The S^{2}MP shows a higher R value than that of the Copernicus SSM. Additionally, the RMSD is lower for the S^{2}MP

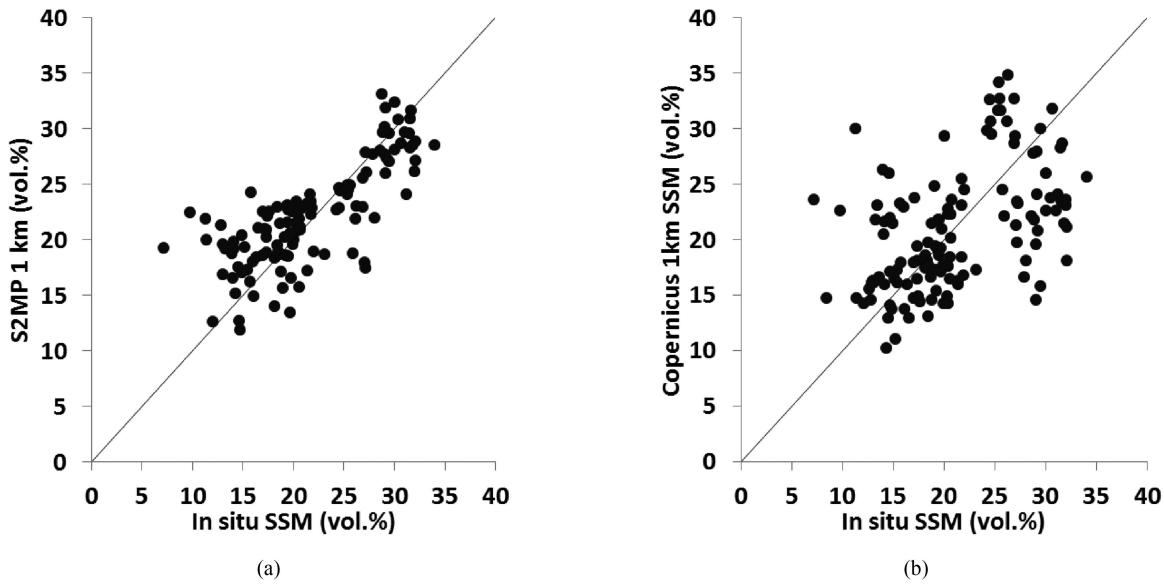

Fig. 3. SSM products against *in situ* measurements. (a) S^2MP-1 km. (b) Copernicus SSM-1 km.

TABLE I
STATISTICS OF THE COMPARISON BETWEEN SSM PRODUCTS AND *in situ* SSM MEASUREMENTS

Product	R	RMSD (vol.%)	Bias (vol.%)	ubRMSD (vol.%)	Sample Size
S^2MP	0.78	4.0	0.52	3.9	122
Copernicus SSM	0.48	6.0	-0.32	6.0	122

than for the Copernicus SSM. Both products show approximate unbiased estimations. However, the bias between *in situ* and satellite soil moisture could be driven from the soil texture maps used for converting dielectric constant in volumetric soil moisture as well as from the accuracy of inversion approaches. Nevertheless, the Copernicus SSM product performs well with an RMSD of approximately 6 vol%. Notably, the p-value of the comparison for both products is lower than 0.01, which indicates that the correlation is significant.

B. Comparison Between S^2MP and C-SSM Products

Fig. 4 represents the maps of statistical metrics calculated from the comparison between the SSM from the S^2MP and C-SSM products during the period between October 2016 and October 2017. Fig. 4(a) represents the correlation coefficient *R* between the two products, Fig. 4(b) represents the RMSD values, Fig. 4(c) shows the bias values (C-SSM - S^2MP), and Fig. 4(d) shows the ubRMSD values over the Occitanie region. Moderate-to-high correlation values between the compared products are observed, mainly in the western, middle, and eastern parts of Occitanie (*R* between 0.5 and 0.9). Fig. 4(b) shows that the RMSD values for these parts are approximately homogeneous and ranging between 4 and 6 vol%. The ubRMSD [see Fig. 4(d)] for these parts show also low values. Between these parts, only the eastern part shows high positive bias values (between 2 and 4 vol%). The correlation map [see Fig. 4(a)] shows low values mainly in the northern part of Occitanie, with moderate RMSD values (between 6 and 8 vol%). High RMSD values (more than 8 vol%) are observed for the northeastern part. The bias map for the northern area shows high positive values [see Fig. 4(c)]. The ubRMSD is generally homogeneous over the Occitanie, with values ranging between 3 and 7 vol%. Notably, the fringes observed in the maps are due to the heterogeneity of the SSM estimates in the C-SSM product at the borders of the subswath, as illustrated in Section II-D. The great difference in SSM values observed at the limit of the subswath induces a difference of bias values between two adjacent areas at the limit of the subswath (case of far western part in *R*, bias and ubRMSD maps).

For some Copernicus cells (1 km $\times$ 1 km), only a small number of S^2MP pixels are sometimes used for calculating the average soil moisture estimation from S^2MP. For example, only 8.5% of 1 km $\times$ 1 km cells contain between 20 and 200 S^2MP pixels (the minimum was fixed to 20 pixels) whereas 75% of the 1 km $\times$ 1 km cells contain more than 1000 S^2MP pixels. The correlation between the two products for the cells with low number of S^2MP pixels was analyzed mainly for the cells containing between 20 and 200 S^2MP pixels. Results showed that there are as many low values as high values of the correlation coefficient (*R*) between both products at these cells (the same number of cells with *R* less than 0.3, between 0.3 and 0.5 and with *R* higher than 0.5).

The statistical metrics obtained from the comparison of both SSM products are analyzed as a function of the land cover [see Fig. 1(b)]. The S^2MP product provides soil moisture estimation

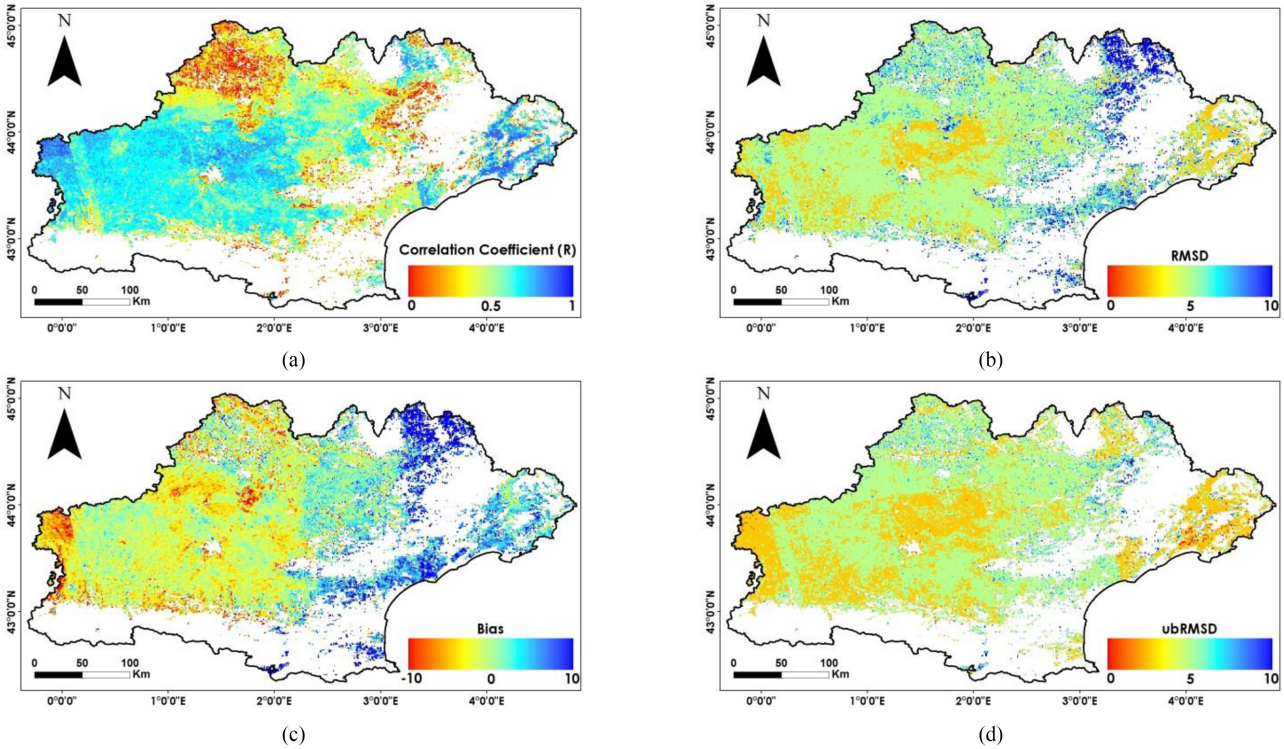

Fig. 4. Statistical metrics maps at 1-km grid generated from the comparison between the C-SSM and S^{2}MP over the Occitanie region. (a) Correlation coefficient R map, (b) RMSD map, (c) bias map, and (d) ubRMSD map.

over agricultural crop land only grown in summer and winter (urban, forest, grassland, and vineyards are masked), which should be considered before analyzing the effect of the land cover. Thus, we suppose that the soil moisture calculated from the S^{2}MP product is the same for the whole cell of 1 km $\times$ 1 km (not composed only of crops). The results reveal that the western and middle parts show the highest R values with smallest bias and RMSD values. In the land cover map, this area shows a majority of summer and winter crops (more than 65% of the area). The eastern part that shows high correlation values but moderate-to-high bias values is composed of a mix of vineyards (30%), grassland (30%), and summer–winter crops (14%). The northern part, with the lowest R and moderate RMSD and bias values, is generally occupied with a mix of grassland (60% of the area) and forests (23% of the area). This part comprises no more than 9% agricultural areas. Finally, the northeastern part (high RMSD and bias values) is mostly covered by a mix of forests (40%) and grassland (40%).

Fig. 5 shows the scatter plots for the comparison between the C-SSM and S^{2}MP over four different cells (each of 1 km $\times$ 1 km) with four different land cover types. Fig. 5(a) shows the scatter plot comparison over a cell with mainly grasslands (89% grassland and 6% summer crops). The comparison indicates low correlation ($R = 0.2$) but moderate RMSD value (7.6 vol%) and unbiased estimation. Fig. 5(b) shows the scatter plot for a cell covered with mainly agricultural areas (80% summer and winter crops and 5% grassland). In this case, the C-SSM and S^{2}MP are highly correlated ($R = 0.8$, RMSD = 4.6 vol%, bias = 1 vol%). This result confirms the evaluation results obtained in Section III-A, where both the C-SSM and S^{2}MP show good agreement with *in situ* measurements over agricultural areas. Fig. 5(c) shows the SSM estimations of both products over a cell with mainly forests (86% forests and 7% summer crops). In this cell, the overestimation of C-SSM with respect to the S^{2}MP is visible (bias = 8 vol%). In fact, over forests, the backscattered signal in C-band is highly affected by the forest canopy because the penetration of the SAR signal to the ground surface is very low. High backscattering coefficients that are observed in the forest could induce high soil moisture estimations in C-SSM and thus an overestimation of SSM by the C-SSM product. Similarly, Fig. 5(d) shows the intercomparison at a cell with a mix of agricultural and vineyard areas (75% vineyards and 18% summer crops) with high bias values, where the C-SSM highly overestimates the S^{2}MP. High biased values over vineyards (5.6 vol%) are due to the high backscattering signal reflected from metals and wooden stakes that are usually present in vineyards. Baghdadi *et al.* [29] demonstrated that vineyards have strong radar backscattering signal because of these stakes. This strong backscattering signal, which is not related to the soil contribution, could induce higher soil moisture estimations.

The analysis of the SSM products' quality according to land cover type reveals that over areas mainly used for cereals and market gardening (the case of the middle and western parts), the correlation between the SSM products is high, indicating high consistency in soil moisture estimation between the products. When the area becomes more occupied by grassland (the case in the northern part), the correlation decreases but keeps moderate

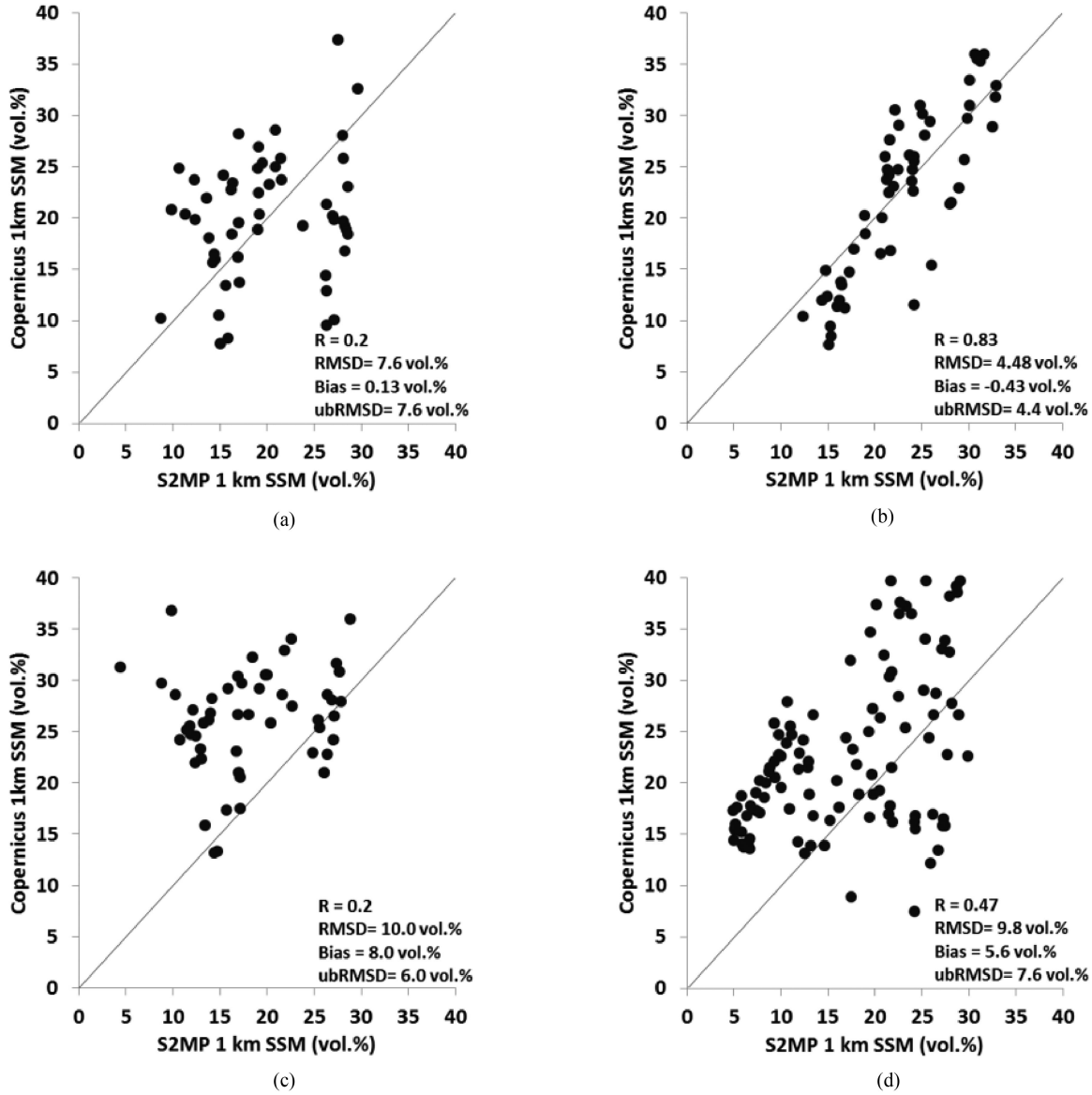

Fig. 5. C-SSM against S^2MP over cell of 1 km × 1 km for (a) mainly grassland (89%), (b) mainly agricultural areas (80% summer and winter crops), (c) mainly forests (86%), and (d) mainly vineyards (75%).

RMSD and bias values. However, when the forested area dominates and the land cover becomes more heterogeneous (forests, grassland, agricultural, etc.) (the case in the northeastern part), an overestimation of C-SSM with respect to S^2MP is observed. Moreover, when the vineyards are dominant in the land cover (the case of the eastern part), overestimation of C-SSM with respect to S^2MP is observed. The limitation observed over heterogeneous land cover for the C-SSM product could be related to the spatial resolution because the product is produced at a 1-km pixel size and not at a fine scale.

C. Temporal Behavior of SSM Series

The temporal evolution of the soil moisture values was investigated over two cells $(1\,\text{km} \times 1\,\text{km})$: one totally covered with winter wheat cultivation [see Fig. 6(a)] near Montpellier, France, and the second with summer maize cultivation in the western part near Tarbes, France [see Fig. 6(b)]. For the wheat cell, *in situ* soil moisture values are also available. Unfortunately, *in situ* measurements are not available over the maize cell of the western part. In addition to S^2MP and C-SSM estimates, the NDVI values derived from Sentinel-2 temporal series images and averaged over the 1-km grid cell were also plotted. The precipitation amounts derived from a local metrological station near each cell [local station in Montpellier for Fig. 6(a) and local station in Tarbes for Fig. 6(b)] were used to qualitatively analyze the behavior of the SSM products. The temporal resolution of the C-SSM is also higher than that of the S^2MP; thus, more points are obtained for the C-SSM product. As mentioned before, the correlation coefficient could only be calculated for soil moisture values of the common estimation dates. For both land cover types, the correlation coefficient between the SSM

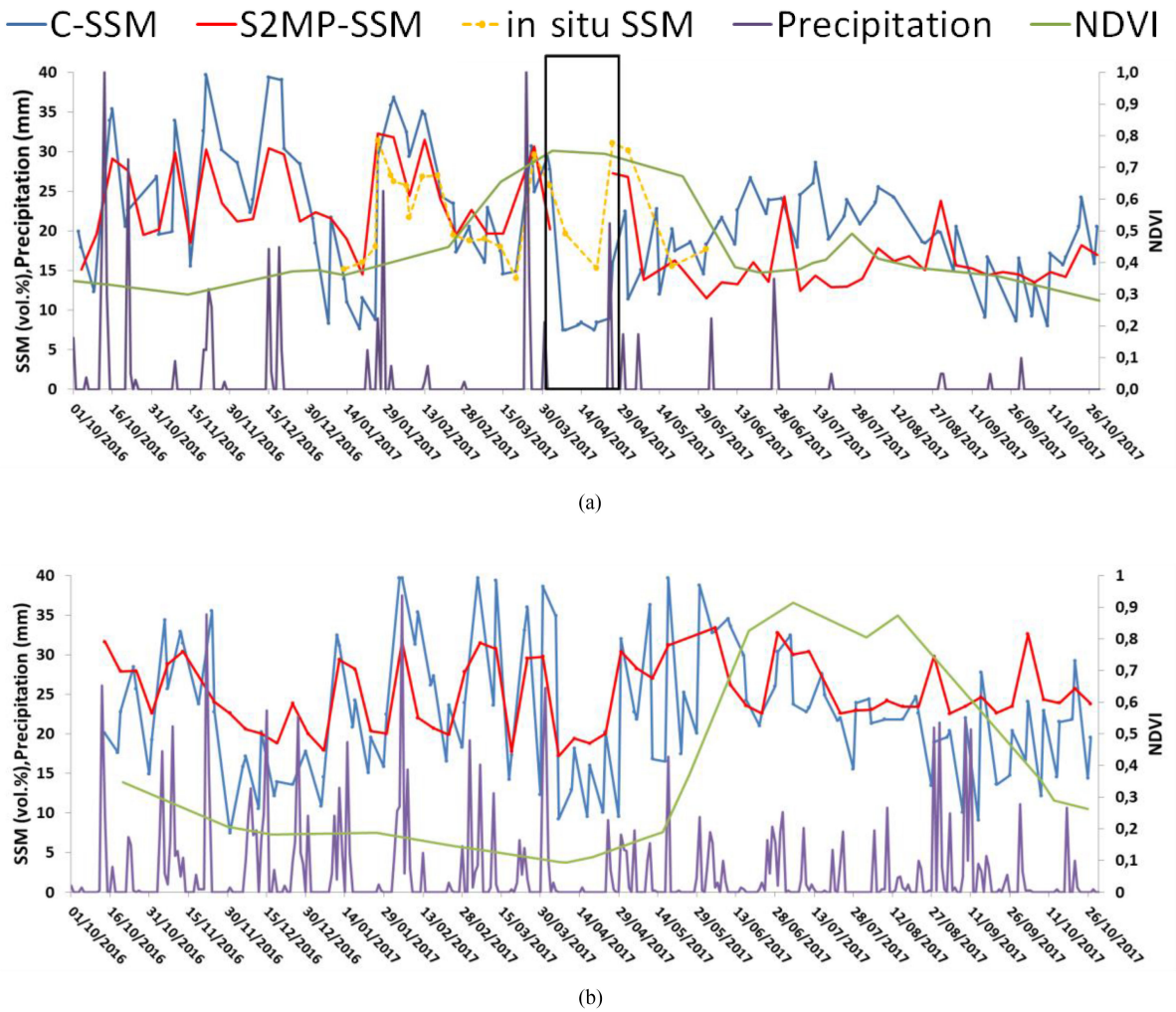

Fig. 6. Temporal series of SSM values derived from C-SSM and S^{2}MP products over (a) winter wheat cultivation cell and (b) summer maize cultivation cell.

products is significant (0.63 for maize and 0.77 for wheat). For the maize cell, the RMSD value is of 5.7 vol%, whereas that of the wheat is 5.2 vol%. Moreover, both products show a consistency with the precipitation events. After a precipitation event, high soil moisture values are estimated in both products (in both maize and wheat cases). However, the C-SSM values frequently show very high SSM values following rainfall events, and the estimation reaches 100% in relative soil moisture (39.7 vol% in volumetric soil moisture). Following a dry period, both products show low soil moisture values, thus expressing dry soil conditions.

An important point in the temporal series concerns the winter wheat cultivation. During the period between March 30, 2017 and April 29, 2017 [black box in Fig. 6(a)], the C-SSM fails to estimate accurate soil moisture values. The relative soil moisture obtained from the C-SSM product is approximately 0% during this period (which corresponds to volumetric soil moisture of approximately 7.5 vol%). When comparing these values to the *in situ* soil moisture measurement, we find that C-SSM abruptly drops down and underestimates the soil moisture. For the same period, the S^{2}MP does not provide any SSM estimation (gap in the red curve). This is due to the fact that over dense vegetation (the case of the wheat with NDVI > 0.7), the soil contribution in the SAR signal in C-band becomes negligible, and the estimation of soil moisture could not be obtained. El Hajj *et al.* [30] studied the penetration of C-band SAR data over wheat, maize, and grassland. They showed that the C-band in VV polarization is not able to penetrate the wheat canopy when the vegetation is well developed (NDVI > 0.7). As a result, the estimation of the SSM values is not reliable. For this reason, in the S^{2}MP algorithm, a mask was applied to eliminate those likely unreliable SSM values for NDVI greater than 0.7 and SSM estimations that are less than 5 vol%.

For the maize canopy [see Fig. 6(b)], both products are able to estimate the soil moisture values, even with well-developed vegetation. For example, between the end of July and the end of August, the NDVI remains high (approximately > 0.8), and both products are able to show reliable SSM values. The SSM values decrease during a time span without rainfall events and increase following a rainfall event, even when the canopy is well developed. However, both El Hajj *et al.* [30] and Joseph *et al.* [31] reported that the soil contribution to the C-band backscattering is

notable when the maize canopy is well developed due to the high order scattering along the soil-vegetation pathway that contains the soil contribution.

IV. Conclusion

The aim of this study was to assess the accuracy of SSM in southern France estimated by the Sentinel-1/Sentinel-2-derived S^2MP and the new C-SSM product at 1-km scale. Using *in situ* measurements, the accuracy of each product was first evaluated and determined by the Pearson correlation coefficient (R), the RMSD, the bias, and the ubRMSD. Then, an intercomparison between the products was performed for one year (between October 2016 and October 2017) over the entire Occitanie region, South France. The results of the intercomparison were further discussed as a function of the land cover. The results reveal that both products show good reliability with *in situ* measurements. However, S^2MP shows higher accuracy (RMSD $=$ 4.0 vol%, $R = 0.77$) than the C-SSM (RMSD $=$ 6.0 vol%, $R = 0.48$) when compared to *in situ* measurements over agricultural areas and grasslands. The analysis of the intercomparison between the products as a function of the land cover shows that the S^2MP and C-SSM are highly correlated over dense agricultural areas (mainly cereals of winter and summer). When the land cover becomes more heterogeneous (mix of forests, grassland, and vineyards with agricultural areas), the correlation between the products decreases. The C-SSM tends to overestimate SSM values over cells containing vineyards and forests. In addition, the C-SSM sometimes shows underestimated SSM values when the vegetation is well developed. In wheat areas, the underestimation is approximately 7.5 vol% when NDVI is greater than 0.7. On the other hand, the algorithm of S^2MP eliminates likely unreliable SSM values for NDVI greater than 0.7 because the SSM estimations in this case are less than 5 vol%.

References

[1] E. Tebbs, F. Gerard, A. Petrie, and E. De Witte, "Emerging and potential future applications of satellite-based soil moisture products," in *Satellite Soil Moisture Retrieval*. New York, NY, USA: Elsevier, 2016, pp. 379–400.

[2] F. Herrmann *et al.*, "Simulation of future groundwater recharge using a climate model ensemble and SAR-image based soil parameter distributions—A case study in an intensively-used Mediterranean catchment," *Sci. Total Environ.*, vol. 543, pp. 889–905, Feb. 2016.

[3] H. Sellami, I. La Jeunesse, S. Benabdallah, N. Baghdadi, and M. Vanclooster, "Uncertainty analysis in model parameters regionalization: A case study involving the SWAT model in Mediterranean catchments (southern France)," *Hydrol. Earth Syst. Sci.*, vol. 18, pp. 2393–2413, 2014.

[4] Q. Gao, M. Zribi, M. Escorihuela, N. Baghdadi, and P. Segui, "Irrigation mapping using Sentinel-1 time series at field scale," *Remote Sens.*, vol. 10, no. 9, Sep. 2018, Art. no. 1495.

[5] M. El Hajj *et al.*, "Soil moisture retrieval over irrigated grassland using X-band SAR data," *Remote Sens. Environ.*, vol. 176, pp. 202–218, Apr. 2016.

[6] N. N. Baghdadi, M. El Hajj, M. Zribi, and I. Fayad, "Coupling SAR C-band and optical data for soil moisture and leaf area index retrieval over irrigated grasslands," *IEEE J. Sel. Topics Appl. Earth Observ. Remote Sens.*, vol. 9, no. 3, pp. 1229–1243, Mar. 2016.

[7] S. Bousbih *et al.*, "Soil moisture and irrigation mapping in a semi-arid region, based on the synergetic use of Sentinel-1 and Sentinel-2 data," *Remote Sens.*, vol. 10, no. 12, Dec. 2018, Art. no. 1953.

[8] K. S. Chen, T.-D. Wu, L. Tsang, Q. Li, J. Shi, and A. K. Fung, "Emission of rough surfaces calculated by the integral equation method with comparison to three-dimensional moment method simulations," *IEEE Trans. Geosci. Remote Sens.*, vol. 41, no. 1, pp. 90–101, Jan. 2003.

[9] A. K. Fung, *Microwave Scattering and Emission Models and Their Applications*. Boston, MA, USA: Artech House, 1994.

[10] N. Baghdadi *et al.*, "A new empirical model for radar scattering from bare soil surfaces," *Remote Sens.*, vol. 8, no. 11, Nov. 2016, Art. no. 920.

[11] P. C. Dubois, J. Van Zyl, and T. Engman, "Measuring soil moisture with imaging radars," *IEEE Trans. Geosci. Remote Sens.*, vol. 33, no. 4, pp. 915–926, Jul. 1995.

[12] S. Paloscia, S. Pettinato, E. Santi, C. Notarnicola, L. Pasolli, and A. Reppucci, "Soil moisture mapping using Sentinel-1 images: Algorithm and preliminary validation," *Remote Sens. Environ.*, vol. 134, pp. 234–248, Jul. 2013.

[13] N. Baghdadi, N. Holah, and M. Zribi, "Calibration of the integral equation model for SAR data in C-band and HH and VV polarizations," *Int. J. Remote Sens.*, vol. 27, no. 4, pp. 805–816, Feb. 2006.

[14] N. Baghdadi, J. A. Chaaya, and M. Zribi, "Semiempirical calibration of the integral equation model for SAR data in C-band and cross polarization using radar images and field measurements," *IEEE Geosci. Remote Sens. Lett.*, vol. 8, no. 1, pp. 14–18, Jan. 2011.

[15] E. P. W. Attema and F. T. Ulaby, "Vegetation modeled as a water cloud," *Radio Sci.*, vol. 13, no. 2, pp. 357–364, Mar. 1978.

[16] B. He, M. Xing, and X. Bai, "A synergistic methodology for soil moisture estimation in an alpine prairie using radar and optical satellite data," *Remote Sens.*, vol. 6, no. 11, pp. 10966–10985, Nov. 2014.

[17] F. Mattia *et al.*, "Sentinel-1 high resolution soil moisture," in *Proc. IEEE Int. Geosci. Remote Sens. Symp.*, Fort Worth, TX, USA, 2017, pp. 5533–5536.

[18] J. Van Doninck, J. Peters, H. Lievens, B. De Baets, and N. E. C. Verhoest, "Accounting for seasonality in a soil moisture change detection algorithm for ASAR Wide Swath time series," *Hydrol. Earth Syst. Sci.*, vol. 16, no. 3, pp. 773–786, Mar. 2012.

[19] Q. Gao, M. Zribi, M. Escorihuela, and N. Baghdadi, "Synergetic use of Sentinel-1 and Sentinel-2 data for soil moisture mapping at 100 m resolution," *Sensors*, vol. 17, no. 9, Sep. 2017, Art. no. 1966.

[20] D. Entekhabi *et al.*, "The soil moisture active passive (SMAP) mission," *Proc. IEEE*, vol. 98, no. 5, pp. 704–716, Mar. 2010.

[21] W. Wagner *et al.*, "The ASCAT soil moisture product: A review of its specifications, validation results, and emerging applications," *Meteorol. Zeitschrift*, vol. 22, no. 1, pp. 5–33, Feb. 2013.

[22] Y. H. Kerr, P. Waldteufel, J.-P. Wigneron, J. Martinuzzi, J. Font, and M. Berger, "Soil moisture retrieval from space: The soil moisture and ocean salinity (SMOS) mission," *IEEE Trans. Geosci. Remote Sens.*, vol. 39, no. 8, pp. 1729–1735, Aug. 2001.

[23] M. El Hajj, N. Baghdadi, M. Zribi, and H. Bazzi, "Synergic use of Sentinel-1 and Sentinel-2 images for operational soil moisture mapping at high spatial resolution over agricultural areas," *Remote Sens.*, vol. 9, no. 12, Dec. 2017, Art. no. 1292.

[24] B. Bauer-Marschallinger *et al.*, "Toward global soil moisture monitoring with Sentinel-1: Harnessing assets and overcoming obstacles," *IEEE Trans. Geosci. Remote Sens.*, vol. 57, no. 1, pp. 520–539, Jan. 2019.

[25] J. Inglada, A. Vincent, M. Arias, B. Tardy, D. Morin, and I. Rodes, "Operational high resolution land cover map production at the country scale using satellite image time series," *Remote Sens.*, vol. 9, no. 1, Jan. 2017, Art. no. 95.

[26] N. Baghdadi, M. El Hajj, M. Zribi, and S. Bousbih, "Calibration of the water cloud model at C-band for winter crop fields and grasslands," *Remote Sens.*, vol. 9, no. 9, Sep. 2017, Art. no. 969.

[27] N. Baghdadi, H. Bazzi, M. El Hajj, and M. Zribi, "Detection of frozen soil using Sentinel-1 SAR data," *Remote Sens.*, vol. 10, no. 8, Aug. 2018, Art. no. 1182.

[28] R. Amri, M. Zribi, Z. Lili-Chabaane, W. Wagner, and S. Hasenauer, "Analysis of C-band scatterometer moisture estimations derived over a semiarid region," *IEEE Trans. Geosci. Remote Sens.*, vol. 50, no. 7, pp. 2630–2638, Jul. 2012.

[29] N. Baghdadi, N. Holah, P. Dubois-Fernandez, X. Dupuis, and F. Garestier, "Evaluation of polarimetric L- and P-bands RAMSES data for characterizing Mediterranean vineyards," *Can. J. Remote Sens.*, vol. 32, no. 6, pp. 380–389, Dec. 2006.

[30] M. El Hajj, N. Baghdadi, H. Bazzi, and M. Zribi, "Penetration analysis of SAR signals in the C and L bands for wheat, maize, and grasslands," *Remote Sens.*, vol. 11, no. 1, Jan. 2018, Art. no. 31.

[31] A. T. Joseph, R. Van Der Velde, P. E. O'Neill, R. Lang, and T. Gish, "Effects of corn on C- and L-band radar backscatter: A correction method for soil moisture retrieval," *Remote Sens. Environ.*, vol. 114, no. 11, pp. 2417–2430, Nov. 2010.

Hassan Bazzi received the master's degree in geomatics in 2018 from AgroParisTech, Montpellier, France, where he is currently working toward the Ph.D. degree with TETIS Research Unit focusing on radar and optical techniques for water resource management in agricultural area.

Nicolas Baghdadi received the Ph.D. degree from the University of Toulon, Toulon, France, in 1994.

From 1995 to 1997, he was a Postdoctoral Researcher with INRS ETE—Water Earth Environment Research Centre, Quebec University, Canada. From 1998 to 2008, he was with French Geological Survey (BRGM), Orléans, France. Since 2008, he has been a Senior Scientist with the National Research Institute of Science and Technology for Environment and Agriculture, Montpellier, France. He is currently the Scientific Director of the THEIA Land Data Centre. His research activities are involved in the areas of microwave remote sensing, image processing, and analysis for satellite and airborne remote sensing data. His main field of interest is the analysis of SAR data and the retrieval of soil parameters (surface roughness and moisture content).

Mohammad El Hajj received the Ph.D. degree from the University of AgroParisTech (TETIS Research Unit), Montpellier, France, in 2015.

Since 2016, he has been a Research Engineer with the National Research Institute of Science and Technology for Environment and Agriculture, Montpellier. His main field of interest is the use of remote sensing data for land surface applications.

Mehrez Zribi received the engineering degree in signal processing from the Ecole Nationale Supérieure d'Ingénieurs en Constructions Aéronautiques, Toulouse, France, in 1995, and the Ph.D. degree from the University of Paul Sabatier, Toulouse, in 1998.

In 1995, he joined the CETP Laboratory (IPSL/CNRS), Vélizy, France. He has been with the Centre National de Recherche Scientifique since 2001. In October 2008, he joined CESBIO Laboratory. His research interests include microwave remote sensing applied to hydrology and microwave modeling and instrumentations.

Hatem Belhouchette received the Master of Science degree in irrigation and cropping system from IAM-Bari, Italy, in 1999, and the Ph.D. degree in cropping system sustainability from École Nationale Supérieure Agronomique, Montpellier, France, in 2004.

Since 2003, he has been with IAM-Montpellier Institute, Montpellier, France, as a Lecturer and Researcher of Agricultural Production Systems. He is currently an Associate Professor-Researcher with the Mediterranean Agronomic Institute of Montpellier (CIHEAM-IAMM), Montpellier. His main expertise and interest is the development of operational methods for the assessment, exploration and design of agricultural production systems, both at field and farm levels.